Available online at www.sciencedirect.com
ScienceDirect
International Journal of Mass Spectrometry 267 (2007) 89–97
International Journal of Mass Spectrometry
www.elsevier.com/locate/ijms

One-photon mass-analyzed threshold ionization spectroscopy (MATI) of *cis*-dichloroethylene (*cis*-$C_2H_2Cl_2$): Cation structure determination via Franck–Condon fit

Yong Jin Bae, Myung Soo Kim *

Department of Chemistry, Seoul National University, Seoul 151-742, South Korea

Received 23 October 2006; received in revised form 17 January 2007; accepted 20 February 2007
Available online 23 February 2007

Abstract

A high-quality one-photon mass-analyzed threshold ionization (MATI) spectrum of *cis*-$C_2H_2Cl_2$ was obtained by using vacuum ultraviolet radiation generated by four-wave mixing in Kr. The ionization energy determined from the position of the 0–0 band in the spectrum was 9.6578 ± 0.0006 eV. Ten vibrational fundamentals for the cation were identified. Most of the overtones and combinations could be assigned properly by comparing with the quantum chemical calculation results. The equilibrium geometry of the cation was determined through Franck–Condon fit.

Keywords: MATI; Franck–Condon fit

1. Introduction

Zero kinetic energy (ZEKE) photoelectron spectroscopy [1–7] and mass-analyzed threshold ionization (MATI) spectroscopy [8–10] are useful techniques to measure accurate ionization energies of neutrals and high-resolution vibration-rotation spectra of cations. In these techniques, a neutral is excited to a Rydberg state (high n, low l) lying close to the ionization limit. It is thought that some neutrals in Rydberg states undergo radiationless transition to high n, l, m states, or so-called ZEKE states [11]. Then, neutrals in ZEKE states are ionized by electric field pulse. ZEKE and MATI spectra are obtained by recording the electron and ion currents, respectively, as a function of the excitation energy. In MATI, cations generated by direct photoionization must be removed before pulsed field ionization (PFI) [12]. Use of the spoil field [13] needed for this purpose and use of high PFI voltage are responsible for poorer resolution of MATI than ZEKE. On the other hand, mass selectivity [14] and capability to generate state-selected molecular ions [15,16] are the important advantages of MATI.

Determining the molecular structure in gas phase is far more difficult for ions than neutrals, the main reason being the difficulty to prepare gas phase charged particles in high enough concentration for spectroscopic study. For small molecular ions, emission spectroscopy [17], laser-induced fluorescence spectroscopy [18], microwave spectroscopy [19], etc. have been used to elucidate their structures. Rotationally resolved ZEKE spectroscopy has also been used to determine the structures of small molecular cations with high symmetry [20,21]. As the number of atoms increases and the symmetry gets lowered, structure determination by using the above techniques becomes increasingly difficult.

As a part of our efforts to analyze MATI spectra, which are essentially the vibrational spectra for molecular cations, we calculated the Franck–Condon factors using the molecular geometries, vibrational frequencies and eigenvectors for the neutral and cation obtained by quantum chemical calculations. However, the simulated spectra thus obtained were different, sometimes rather drastically, from the experimental data. Then, we used experimental data for the neutral geometry and the frequencies for the neutral and cation and attempted Franck–Condon fit [22] by treating the cation geometry as an adjustable parameter. For all the cases investigated so far [22,23], the intensity patterns in the MATI spectra could be reproduced satisfactorily through such calculations. Use of the eigenvectors obtained by quantum chemical calculations was unavoidable in this method. However, the cation geometries determined through

* Corresponding author. Tel.: +82 2 880 6652; fax: +82 2 889 1568.
E-mail address: myungsoo@snu.ac.kr (M.S. Kim).

1387-3806/$ – see front matter © 2007 Elsevier B.V. All rights reserved.
doi:10.1016/j.ijms.2007.02.025

the Franck–Condon fit were quite insensitive to the quantum chemical levels used to obtain the eigenvectors. This suggests that the method can be useful for cation structure determination when rotationally resolved spectra are not available. It is to be mentioned that rotational data alone are not sufficient to determine the structure of a large molecule.

In the usual two-photon scheme [24,25] for MATI or ZEKE, the excitation to a Rydberg state occurs via an intermediate state. Hence, calculation of the intensity pattern in such a spectrum requires additional information on the excited state which is not generally available. In this respect, the one-photon MATI scheme [26,27] practiced in this laboratory is especially advantageous for the method of Franck–Condon fit. Avoiding the excited electronic state has other advantages also. For molecules without a UV chromophore, the first excited states cannot be accessed by one-photon absorption with a commercial dye laser. Also, many of these states are dissociative, making two-step excitation difficult.

In this work, a high quality vibrational spectrum for *cis*-$C_2H_2Cl_2^+$ has been obtained with one-photon MATI. The method of Franck–Condon fit has been used to estimate the cation geometry.

2. Experimental

cis-$C_2H_2Cl_2$ was purchased from TCI (Tokyo) and used without further purification. Gaseous sample was seeded in Ar at the stagnation pressure of 2 atm, supersonically expanded through a pulsed nozzle (diameter: 500 μm, General Valve) and introduced to the ionization chamber through a skimmer (diameter: 1 mm, Beam Dynamics) placed about 3 cm downstream from the nozzle orifice. To identify hot bands, He was used as the carrier gas. The background pressure in the ionization chamber was 2×10^{-8} torr.

The method to generate pulsed vacuum ultraviolet (VUV) radiation by four-wave difference frequency mixing in Kr was explained in detail previously and will not be repeated here [28–30]. The VUV laser pulse was collinearly overlapped with the molecular beam in a counterpropagation manner, and slit electrodes were used to collect the ions efficiently. Weak spoil field (1 V/cm) [13] was applied to remove the directly produced ions. To achieve the pulsed field ionization (PFI) [12] of the neutrals in ZEKE states, the electric field of 25 V/cm was applied 15 μs after the VUV pulse. The ions generated were then accelerated, flown through a field-free region, and detected. Scrambling field [13] was applied at the laser irradiation time, which significantly lengthened the lifetime of the ZEKE states. Photoelectric current from a thin gold plate placed in the VUV beam path was used to calibrate the VUV intensity [31].

3. Theory and calculation

3.1. Quantum chemical calculation

Quantum chemical calculations were carried out for the *cis*-$C_2H_2Cl_2$ neutral and cation in the ground electronic states at the Hartree–Fock (HF), the second order Möller–Plesset perturbation theory (MP2) and the density functional theory (DFT) levels using GAUSSIAN 98 suite of programs [32]. The size of the basis set was systematically increased until the basis set dependence became insignificant. Equilibrium geometries, Hessians, vibrational frequencies, and normal mode eigenvectors were obtained for the *cis*-$C_2H_2Cl_2$ neutral and cation.

3.2. Vibrational selection rule

The vibrational selection rule in ZEKE/MATI is essentially the same as that for general electronic transitions derived with the Born–Oppenheimer approximation. Neutrals under the beam condition are mostly in the ground vibrational state, which is totally symmetric (a_1 in the case of *cis*-$C_2H_2Cl_2$). Then, the transitions to the totally symmetric vibrational states of the cation such as the fundamentals and overtones for totally symmetric modes, the even number overtones for nontotally symmetric modes (a_2, b_1, and b_2 in the present case) and totally symmetric combinations are allowed. However, it is known that the transitions to nontotally symmetric states also appear, even though weakly, via vibronic mechanism. Relative intensities of the vibrational peaks due to electric dipole-allowed transitions can be estimated by Franck–Condon calculation, while those due to forbidden transitions are zero under the Born–Oppenheimer approximation.

3.3. Franck–Condon factor

The method of Sharp and Rosenstock [33] which treats vibrations as harmonic was adopted to calculate the Franck–Condon factors. In this method, the geometries, the vibrational frequencies and the normal mode eigenvectors for the initial and final states are needed. The following relation is used to account for the difference in normal coordinate between the initial ($\mathbf{Q}''$) and final ($\mathbf{Q}'$) states.

$$\boldsymbol{Q}'' = \boldsymbol{J}\boldsymbol{Q}' + \boldsymbol{K} \tag{1}$$

From **J** and **K**, the following **C** and **D** matrices are evaluated.

$$\mathbf{C} = 2\boldsymbol{\Gamma}'^{1/2}[\mathbf{J}^{\dagger}\boldsymbol{\Gamma}''\mathbf{J} + \boldsymbol{\Gamma}']^{-1}\boldsymbol{\Gamma}'^{1/2} - \mathbf{1} \tag{2}$$

$$\mathbf{D} = -2\boldsymbol{\Gamma}'^{1/2}[\mathbf{J}^{\dagger}\boldsymbol{\Gamma}''\mathbf{J} + \boldsymbol{\Gamma}']^{-1}\mathbf{J}^{\dagger}\boldsymbol{\Gamma}''\mathbf{K} \tag{3}$$

Here $\boldsymbol{\Gamma}'$ and $\boldsymbol{\Gamma}''$ are diagonal matrices which have the vibrational frequencies of the cation and the neutral, respectively, as the diagonal elements. Then, Franck–Condon factors are evaluated from **C** and **D** as follows.

$$\mathrm{FCF}(i) = \frac{D_i^2}{2}, \qquad i\text{-mode fundamental,} \tag{4}$$

$$\mathrm{FCF}(i,j) = \frac{(2C_{ij} + D_i D_j)^2}{4}, \qquad i, j \text{ modes combination.} \tag{5}$$

In the calculation of the relative intensities of MATI peaks, properties of the cation were assumed to approximate those of the ion core of a high Rydberg state. The internal coordinates were

used to calculate **J** and **K**. These were five bond lengths, CC, two CCl and two CH, four bond angles, two ∠CCCl and two ∠CCH and three dihedral angles, ∠ClCCCl, ∠HCCH and ∠ClCCH.

4. Results and discussion

4.1. Quantum chemical calculation

In all the calculations performed at the HF, MP2 and DFT levels using various basis sets, the neutral and cation of *cis*-$C_2H_2Cl_2$ have been found to be planar with the C_{2v} symmetry. Considering valence orbitals only, the ground state electron configuration of the neutral [34] is ... $(10a_1)^2(9b_2)^2(3b_1)^2$, resulting in the $\tilde{X}^1A_1$ ground electronic state. Here $3b_1$ is a π orbital with C=C bonding and C–Cl antibonding character. Both $9b_2$ and $10a_1$ are chlorine 3p in-plane nonbonding orbitals, $n(\mathrm{Cl3p}_{\parallel})$. Removal of an electron from $3b_1$ results in the ground electronic state of the cation, $\tilde{X}^2B_1$.

The optimized geometries of the neutral and the cation obtained at the B3LYP/6-311++G(3df,3pd) level are listed in Table 1 together with experimental data for the neutral [35]. It is seen that the calculated geometry agrees quite well with the experimental one for the neutral. Geometry changes upon ionization between the calculated results are also listed in Table 1. The C=C bond length is lengthened and the C–Cl bond lengths are shortened upon ionization in agreement with the character of the $3b_1$ orbital losing an electron. In addition ∠CCCl and ∠CCH bond angles decrease slightly. Based on the calculated changes in geometry, one expects to observe strong fundamentals and overtones for the vibrational modes with CC stretching, CCl stretching, CCCl bending and CCH bending characters in the MATI spectrum.

cis-$C_2H_2Cl_2$ has 12 nondegenerate normal modes, ν_1–ν_5 belonging to a_1, ν_6 and ν_7 to a_2, ν_8 to b_1 and ν_9–ν_{12} to b_2 following the Mulliken notation. Calculated vibrational frequencies for the neutral and the cation are listed in Table 2 together with experimental data for the neutral [36]. Among the a_1-type modes, ν_1 is symmetric C–H stretching, ν_2 is C=C stretching, ν_3 is symmetric CCH in-plane bending, ν_4 is symmetric C–Cl stretching and ν_5 is symmetric CCCl in-plane bending. Two a_2-type modes, ν_6 and ν_7, are due to asymmetric out-of-plane bending, respectively, while the lone b_1-type mode, ν_8, is due to symmetric out-of-plane bending. Among the b_2-type modes, ν_9 is asymmetric C–H stretching, ν_{10} is asymmetric CCH in-plane bending, ν_{11} is asymmetric C–Cl stretching and ν_{12} is asymmetric CCCl in-plane bending. As an aid for vibrational assignment, the Franck–Condon factors for the fundamentals normalized to that of the 0–0 band have been calculated using the quantum chemical results, which are listed in the same table. The calculated Franck–Condon factors predict strong fundamentals for the ν_2–ν_5 modes in agreement with the qualitative prediction based on the geometry changes upon ionization.

Table 1
Geometries of the *cis*-$C_2H_2Cl_2$ neutral and cation in the ground electronic states calculated at the B3LYP level using the 6-311++G(3df,3pd) basis set

C_{2v}	Neutral ($\tilde{X}^1A_1$)		Cation ($\tilde{X}^2B_1$)
	Exp.[a]	B3LYP	B3LYP[b]
Interatomic distance (Å)			
C=C	1.337	1.325	1.396 (0.071)
C–Cl	1.717	1.720	1.648 (−0.072)
C–H	1.096	1.079	1.084 (0.005)
Bond angle (°)			
∠CCCl	124.0	125.3	124.5 (−0.8)
∠CCH	120.3	120.4	118.8 (−1.6)
Dihedral angle (°)			
∠ClCCCl	0.0	0.0	0.0
∠ClCCH	180.0	180.0	180.0

[a] The experimental data in [35].
[b] Numbers in the parentheses show the geometrical changes upon ionization between the calculated results.

Table 2
Experimental vibrational frequencies (in cm^{-1}) for the *cis*-$C_2H_2Cl_2$ neutral, those calculated for the neutral and the cation at the B3LYP/6-311++G(3df,3pd) level, and the calculated intensities for the fundamentals

Mode	Symm.	Neutral ($\tilde{X}^1A_1$)		Cation ($\tilde{X}^2B_1$)	
		Exp.[a]	B3LYP	B3LYP	Int.[b]
1	a_1	3077	3224	3192	0.001
2	a_1	1587	1645	1444	0.820
3	a_1	1179	1219	1229	0.356
4	a_1	711	712	801	0.361
5	a_1	173	168	182	0.053
6	a_2	876	906	910	–
7	a_2	406	422	286	–
8	b_1	697	709	738	–
9	b_2	3072	3203	3178	–
10	b_2	1303	1319	1373	–
11	b_2	857	853	959	–
12	b_2	571	577	591	–

[a] IR/Raman spectroscopic data in [36].
[b] Intensities calculated with molecular parameters obtained at the B3LYP/6-311++G(3df,3pd) level. Normalized to the 0–0 band intensity.

4.2. One-photon MATI spectrum and ionization energy

One-photon MATI spectra of *cis*-$C_2H_2Cl_2$ recorded by monitoring $C_2H_2{}^{35}Cl_2^+$, $C_2H_2{}^{35}Cl^{37}Cl^+$ and $C_2H_2{}^{37}Cl_2^+$ generated in the ground electronic state are shown in Fig. 1. Three spectra look virtually the same except for tiny isotopic shifts for some peaks. Spectral acquisition beyond 80,850 cm^{-1} could not be made due to poor VUV intensity.

The most intense peak at around 77,888 cm^{-1} is the 0–0 band, the position of which corresponds to the ionization energy. To determine the accurate ionization energy, its position was measured by using various PFI fields with the spoil field [13] turned off and the results were extrapolated to the zero field limit. The ionization energies thus determined were 9.6578 ± 0.0006, 9.6576 ± 0.0006 and 9.6575 ± 0.0006 eV for $C_2H_2{}^{35}Cl_2$, $C_2H_2{}^{35}Cl^{37}Cl$ and $C_2H_2{}^{37}Cl_2$ isotopomers, respectively. These are in excellent agreement with the PFI-photoelectron (PFI-PE) result reported by Ng and coworkers [37] as listed in Table 3.

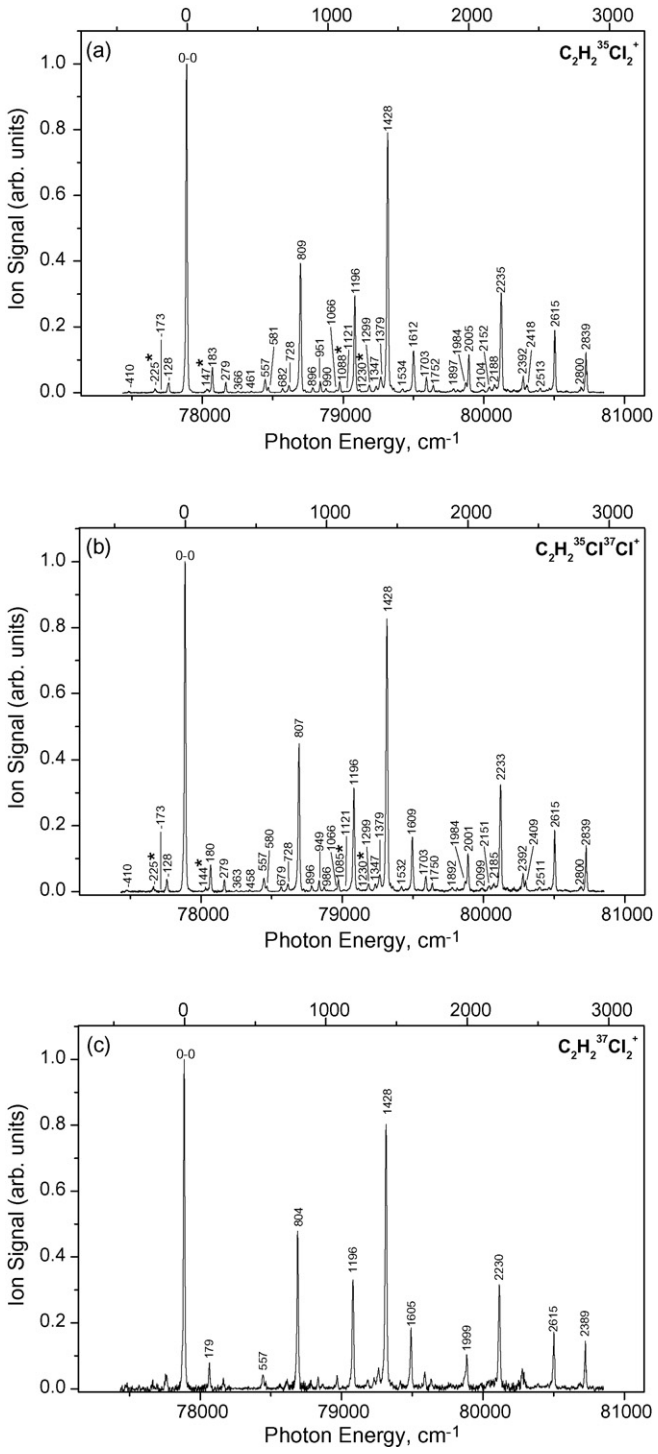

Fig. 1. One-photon MATI spectra of *cis*-$C_2H_2Cl_2$ recorded by monitoring *cis* isomers of (a) $C_2H_2{}^{35}Cl_2{}^+$, (b) $C_2H_2{}^{35}Cl^{37}Cl^+$, and (c) $C_2H_2{}^{37}Cl_2{}^+$ in the ground electronic state. The *x*-scale at the top of the figure corresponds to the vibrational frequency scale for the cation in cm^{-1}. Its origin is at the 0–0 band position. Stars indicate peaks due to the *trans* isomer.

4.3. Vibrational assignment

Assuming that the spoil field affects the positions of all the peaks appearing in the MATI spectrum similarly, the vibrational frequency of the cation corresponding to each peak can be estimated simply by taking the difference of its position from that of the 0–0 band. Vibrational frequency scale with the origin at the 0–0 band position is also shown in Fig. 1. The positions and relative intensities of the peaks appearing in the MATI spectrum of $C_2H_2{}^{35}Cl_2$ are listed in Table 4. Isotopic shifts for C_2H_2 ^{35}Cl $^{37}Cl^+$ are also listed in the same table.

Table 3
Ionization energy (IE) to the ground electronic state of *cis*-$C_2H_2Cl_2$ cation, in eV

	IE($\tilde{X}$)	
cis-$C_2H_2{}^{35}Cl_2$	9.6578 ± 0.0006	This work
cis-$C_2H_2{}^{35}Cl^{37}Cl$	9.6576 ± 0.0006	This work
cis-$C_2H_2{}^{37}Cl_2$	9.6575 ± 0.0006	This work
cis-$C_2H_2Cl_2$	9.65839 ± 0.00025	Ref. [37]

The vibrational spectrum of *cis*-$C_2H_2Cl_2{}^+$ recorded by PFI-PE and its assignment were reported by Ng and coworkers previously [37] (vibrational modes were numbered in order of increasing frequency in their work while the Mulliken notation which takes into account the mode symmetry has been adopted in the present work). Even though the overall agreement between the vibrational spectra obtained by the above PFI-PE and the present MATI technique is good, the present spectrum shows much better resolution and signal-to-noise ratio. Also, the present spectrum covers wider vibrational frequency range (0–2900 cm^{-1}) than the PFI-PE spectrum (0–1500 cm^{-1}). More important is the fact that some of the assignments made by Ng and coworkers look spectroscopically unreasonable. For example, Ng and coworkers assigned the peaks at 181, 277, 424 and 683 cm^{-1} in the PFI-PE spectrum to 5^1, 7^1, 5^17^1 and 5^27^1, respectively. The frequencies of the latter two peaks were substantially different from $181 + 277 = 458$ and $2 \times 181 + 277 = 639$ predicted from the 5^1 and 7^1 positions. In addition, the peak at 683 cm^{-1} appeared prominently while 5^2 was not observed at all in the PFI-PE spectrum. Mediation of the near-resonance autoionization mechanism was invoked by Ng and coworkers to explain the spectral alterations involved in their assignments. Since the quality of our MATI spectrum was far better than the PFI-PE spectrum, we attempted to assign the peaks following the spectroscopic common sense as closely as possible rather than invoking exotic mechanisms to account for irregularities. The guidelines we used are as follows. For frequencies below 1000 cm^{-1}, a plausible assignment was made only when the experimental frequency was within ±20 cm^{-1} from the calculated frequency. The window was widened to ±30 cm^{-1} for peaks above 1000 cm^{-1}. For overtones and combinations, experimental frequencies of the fundamentals or lower overtones and combinations were used to estimate the frequencies of the candidates. The intensity of a peak was also taken into account for a positive assignment. For example, a peak was assigned to 2^14^1 only when its relative intensity was close to the product of the relative intensities of 2^1 and 4^1. Finally, observed isotopic shifts were compared with the calculated shifts. Following these guidelines, a reasonable set of vibrational assignments could be obtained even though some uncertainty remained for very weak peaks. The assignments for

Table 4
Theoretical and experimental (MATI) vibrational frequencies (in cm^{-1}), peak intensities, and their assignments for the *cis*-$C_2H_2Cl_2^+$ in the ground electronic state[a]

Mode	Symm.	Neutral ($\tilde{X}^1A_1$)		Cation ($\tilde{X}^2B_1$)				
		Exp.[b]	B3LYP	Theoretical			MATI	
		Freq.	Freq.[c]	Freq.[c]	Int.[d,e]	Int.[e,f]	Freq.	Int.[e]
Fundamentals								
1	a_1	3077	3224	3192	0.001	0.017		
2	a_1	1587	1645	1444	0.820	0.777	1428	0.791
3	a_1	1179	1219	1229	0.356	0.295	1196	0.295
4	a_1	711	712	801 (−3)	0.361	0.361	809 (−2)	0.393
5	a_1	173	168	182 (−3)	0.053	0.080	183 (−3)	0.077
6	a_2	876	906	910			896	0.015
7	a_2	406	422	286			279	0.032
8	b_1	697	709	738			728	0.015
9	b_2	3072	3203	3178				
10	b_2	1303	1319	1373			1347	0.019
11	b_2	857	853	959 (−3)			951 (−2)	0.034
12	b_2	571	577	591 (−2)			581 (−1)	0.017
Overtones and combinations								
Trans							−225	0.013
Trans							147 (−3)	0.009
5^2				364 (−6)		0.003	366 (−3)	0.005
5^17^1				468 (−3)			461 (−3)	0.005
7^2				572		0.017	557	0.041
5^17^2				754 (−3)		0.001	744 (−2)	0.007
4^15^1				983 (−6)		0.027	990 (−4)	0.014
$4^17^1 + 5^16^1 + trans$							1088	0.035
$5^111^1 + 7^212^1$							1121	0.005
6^17^1				1196		0.007	1173	0.024
Trans							1230	0.009
$3^15^1 + 4^17^2 + 4^112^1$							1379	0.048
8^2				1476		0.001	1453	0.022
3^17^1				1515			1471	0.014
$4^18^1 + 5^110^1 + 11^112^1$							1534	0.012
$4^2 + 2^15^1$							1612	0.127
$2^17^1 + 4^16^1$							1703	0.048
$3^17^2 + 4^111^1$							1752	0.024
$3^112^1 + 10^112^1$							1776	0.006
$2^15^2 + 6^2$							1795	0.006
$4^27^1 + 2^15^17^1 + 11^2$							1897	0.011
3^18^1				1967			1925	0.009
2^17^2				2016		0.013	1984	0.030
$3^14^1 + 2^112^1$							2005	0.116
3^16^1							2104	0.010
$2^18^1 + 4^110^1 + 3^111^1$							2152	0.018
$3^14^15^1 + 4^27^2 + 4^112^1$							2188	0.023
2^14^1				2245 (−3)		0.336	2235 (−2)	0.301
$3^14^17^1$				2316 (−3)			2282 (−3)	0.009
2^16^1				2354			2324	0.007
3^2				2458		0.045	2392	0.051
$2^14^15^1 + 4^3$							2418	0.024
$2^14^17^1$				2531 (−3)			2513 (−2)	0.014
3^110^1				2602			2535	0.006
$2^15^111^1 + 3^14^17^2$							2559	0.009
$3^25^1 + 3^14^112^1 + 4^211^1$							2578	0.015
2^13^1				2673		0.199	2615	0.190
$3^14^2 + 2^13^15^1 + 2^14^17^2 + 2^14^112^1$							2800	0.017
2^2				2888		0.123	2839	0.123
Hot bands								
$7^0 \leftarrow 7^1$				−406			−410	0.005
$7^1 \leftarrow 7^1$				−120			−128	0.028
$4^17^1 \leftarrow 7^1$				681			682(−3)	0.014
$3^17^1 \leftarrow 7^1$				1109			1066	0.008

Table 4 (*Continued*)

Mode	Symm.	Neutral ($\tilde{X}^1A_1$)		Cation ($\tilde{X}^2B_1$)				
		Exp.[b]	B3LYP	Theoretical			MATI	
		Freq.	Freq.[c]	Freq.[c]	Int.[d,e]	Int.[e,f]	Freq.	Int.[e]
$2^1 7^1 \leftarrow 7^1$				1324			1299	0.023
$2^1 4^1 7^1 \leftarrow 7^1$				2125			2104	0.010
$2^1 3^1 7^1 \leftarrow 7^1$				2553			2486	0.006

[a] Numbers in parentheses are isotopic shifts for $C_2H_2{}^{35}Cl^{37}Cl^+$.
[b] IR/Raman spectroscopic data in [36].
[c] B3LYP/6-311++G(3df,3pd) results.
[d] Intensities calculated with molecular parameters obtained at the B3LYP/6-311++G(3df,3pd) level.
[e] Normalized to that of the 0–0 band.
[f] Determined via Franck–Condon fit. See text for details.

the fundamentals are rather similar to those reported by Ng and coworkers while those for the overtones and combinations are significantly different. Table 4 shows the assignments for the peaks, some details of which will be described below.

Since the purity of the *cis*-$C_2H_2Cl_2$ sample is 99% only, MATI peaks due to contaminants may appear in the MATI spectrum. The most important of these contaminants is *trans*-$C_2H_2Cl_2$ whose ionization energy is smaller than that of the *cis* isomer by $219 \pm 10\,cm^{-1}$. The 0–0 band of the *trans* isomer can be readily identified as the peak at $-225\,cm^{-1}$ in the MATI spectrum of the *cis* isomer, Fig. 1(a). Then, other *trans* peaks present in the spectrum were identified by utilizing the MATI spectral data reported previously [22]. Accordingly, the peaks at 147 and 1230 cm^{-1} were found to be entirely due to the *trans* contaminant. Even though the peaks at 728 and 1088 cm^{-1} appeared at strong *trans* peak positions, their intensities were larger than predicted from the *trans* spectral pattern. In these cases, both *trans* and *cis* isomers must have contributed to the intensities at these positions. Other *trans* peaks were weaker and did not affect the assignment for the *cis* isomer. We also identified transitions from excited vibrational states of the neutral, or hot bands, by changing the carrier gas and beam expansion condition. These were the peaks at −410, −128, 682, 1066, 1299, 2104 and 2486 cm^{-1}. It is to be noted that most of these appeared at around 128 cm^{-1} lower frequencies than the major peaks in the spectrum. The peak at −410 and $-128\,cm^{-1}$ could be assigned to $7^0 \leftarrow 7^1$ and $7^1 \leftarrow 7^1$ based on the calculated ν_7 frequencies of 422 and 286 cm^{-1}, respectively, for the neutral and cation. Other peaks were combinations involving 7^1. The major hot band at $-128\,cm^{-1}$ was not identified by Ng and coworkers. Accordingly, the assignments for the above combinations were erroneous, which led to erroneous assignments for other peaks in their work. Since the frequency of ν_5 is lower than that of ν_7 in the neutral, one expects to observe the $5^0 \leftarrow 5^1$ and $5^1 \leftarrow 5^1$ hot bands also. The latter band was difficult to identify because it overlapped with the strong 0–0 band. The former band was observed at $-173\,cm^{-1}$. Its intensity was weaker than expected.

Using the calculated frequencies and Franck–Condon factors, four strong peaks at 1428, 1196, 809, and 183 cm^{-1} could be assigned to 2^1, 3^1, 4^1, and 5^1, respectively. Presence of several strong fundamentals in the low-frequency range means that their overtones and combinations will appear at higher frequency. Accordingly, the peaks at 2839, 2392, 1612 and 366 cm^{-1} could be assigned to the overtones 2^2, 3^2, 4^2 and 5^2, respectively. Also the peaks at 2615, 2235, 2005, 1612, 1379 and 990 cm^{-1} were assigned to the combinations $2^1 3^1$, $2^1 4^1$, $3^1 4^1$, $2^1 5^1$, $3^1 5^1$ and $4^1 5^1$, respectively.

Following our assignment of the peak at $-128\,cm^{-1}$ to $7^1 \leftarrow 7^1$, the peak at $279\,cm^{-1}$ was assigned to 7^1. Its position is close to $286\,cm^{-1}$ calculated at the DFT level. Considering that the same fundamental appears at $406\,cm^{-1}$ for the neutral, $7^1 \leftarrow 7^1$ is expected at $279 - 406 = -127\,cm^{-1}$ in agreement with its observation at $-128\,cm^{-1}$. Then, the hot bands left unassigned, namely those at 682, 1066, 1299, 2104 and 2486 cm^{-1} could be assigned to $4^1 7^1 \leftarrow 7^1$, $3^1 7^1 \leftarrow 7^1$, $2^1 7^1 \leftarrow 7^1$, $2^1 4^1 7^1 \leftarrow 7^1$ and $2^1 3^1 7^1 \leftarrow 7^1$, respectively. Overtones and combinations including ν_7 and ν_2–ν_5 were $5^1 7^1$, 7^2, $5^1 7^2$, $3^1 7^1$, $2^1 7^2$, $3^1 4^1 7^1$ and $2^1 4^1 7^1$ at 461, 557, 744, 1471, 1984, 2282 and 2513 cm^{-1}, respectively.

After assigning the above peaks, the fundamentals of the asymmetric vibrations, which are electric dipole-forbidden could be identified. These were 6^1, 8^1, 10^1, 11^1 and 12^1 at 896, 728, 1347, 951 and 581 cm^{-1}, all appearing near the calculated frequencies. Overtones and combinations involving the asymmetric vibrations could be assigned also. The results are listed in Table 4. It is to be mentioned that all the assignments could be made in accordance with the spectroscopic common sense. Proper assignments could not be made only for some of very weak peaks such as those appearing at 842 and 2704 cm^{-1}. Namely, no evidence could be found which indicated severe alteration in frequency and intensity due to the participation of the autoionization and channel interaction mechanisms [11,38,39].

4.4. Franck–Condon fit

It is known that the relative intensities of vibrational peaks in an electronic absorption spectrum are well represented by the Franck–Condon factors. Namely, the absorption spectrum simulated with calculated Franck–Condon factors would resemble the experimental spectrum as far as the molecular parameters used in the calculation are correct. In the case of ZEKE and MATI, transitions occur to Rydberg states. Since each rovibrational state of a cation has its own quasi-continuum of

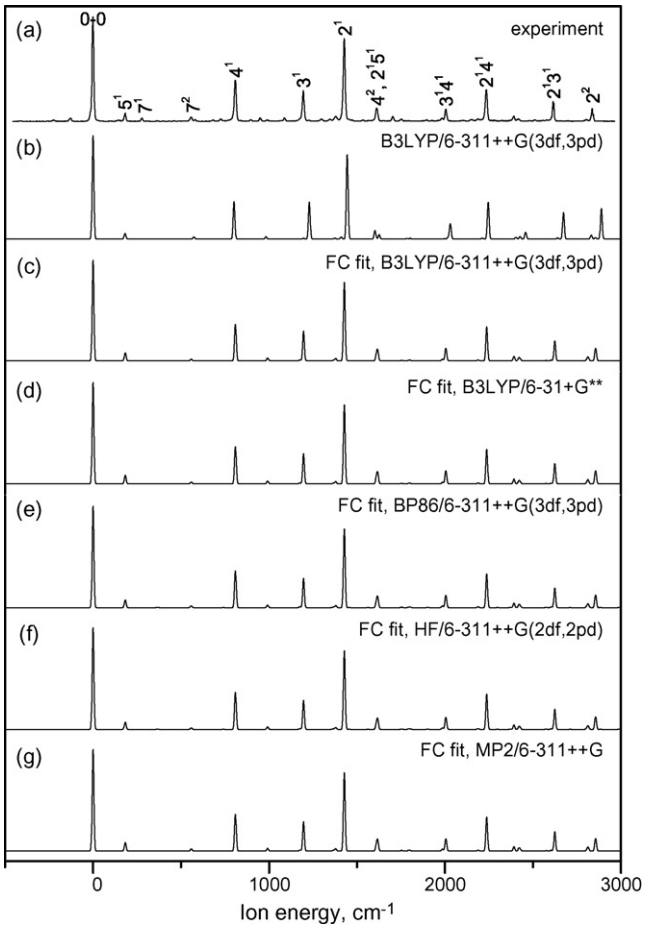

Fig. 2. (a) One-photon MATI spectrum of *cis*-$C_2H_2Cl_2$. (b) A spectrum simulated by using the Franck–Condon factors calculated with the molecular parameters obtained at the B3LYP/6-311++G(3df,3pd). The simulated spectra obtained via Franck–Condon fit (see text for details) using experimental data and eigenvectors calculated at the B3LYP/6-311++G(3df,3pd), B3LYP/6-31 + G**, BP86/6-311++G(3df,3pd), HF/6-311++G(2df,2pd), and MP2/6-311++G are shown in (c), (d), (e), (f), and (g), respectively.

Rydberg states and those leading to different ro-vibrational states may mix, a ZEKE/MATI peak may gain intensity from Rydberg transitions to higher ro-vibrational states. Intensity alteration due to this channel interaction [11,38,39] has been reported for some systems. A careful comparison between the experimental and simulated spectra is needed to check the participation of this mechanism.

We first calculated the Franck–Condon factors calculated using the geometries, vibrational frequencies, and eigenvectors of the *cis*-$C_2H_2Cl_2$ neutral and cation obtained by quantum chemical calculations. The spectrum simulated with the Franck–Condon factors calculated by the parameters obtained at the B3LYP/6-311++G(3df,3pd) level is compared with the experimental MATI spectrum in Fig. 2. Number of peaks in the simulated spectrum is much less than that in the experimental spectrum because only the peaks due to the allowed transition appear in the former spectrum. Other than this difference, the intensity pattern in low frequency range of the experimental spectrum is rather similar to that in the simulated spectrum. Namely, the low frequency peaks including the 0–0 band do not seem to gain intensity via channel interaction. For example, the intensity of the 3^1 fundamental in the experimental spectrum is a little smaller than in the simulated spectrum. Even though the intensities of the high frequency peaks in the experimental spectrum are a little lower than in the simulated spectrum, their relative intensities display regular pattern. For example, the $3^14^1{:}2^14^1$ intensity ratio is similar to the $3^1{:}2^1$ ratio and $2^14^1{:}2^13^1$ is similar to $4^1{:}3^1$. This led us to conclude that the mismatch between the experimental and simulated intensity patterns was not due to channel interaction but probability due to the inaccuracy of the molecular parameters used in the Franck–Condon factor calculation, which were obtained by quantum chemical method.

For rigorous comparison between the experimental and calculated intensity patterns, it is necessary to calculate Franck–Condon factors by using experimental molecular parameters or accurate ground state potential energy surfaces both for the neutral and for the cation. The experimental data for the ground state geometry and vibrational frequencies of the *cis*-$C_2H_2Cl_2$ neutral are available from the literature and the experimental vibrational frequencies of the cation have been obtained in the present work. Then, the remaining difficulties are in obtaining the ground state geometry of the cation and the eigenvectors for the neutral and cation. In our previous works [22], eigenvectors for the neutral and cation obtained at various quantum chemical levels were used and the level-dependence in the final results was checked. Finally, the cation geometrical parameters were treated as variables and were changed systematically attempting to achieve a good fit between the experimental and simulated spectral patterns in the low-frequency region.

We attempted to reproduce the experimental intensity patterns for the fundamentals and other peaks in the low frequency range by varying the geometry of the cation. Among the geometrical parameters of the cation, those obtained by quantum chemical calculations were used for the C–H bond lengths because the C–H stretching peaks were not measured and hence further adjusting them was meaningless. Even after the best attempt to fit, the simulated intensity of 2^2 was stronger than the experimental intensity. As a further attempt to reproduce the intensity of this peak, we varied the C_{22} element of the **C** matrix in Eq. (2), arriving at a good fit at C_{22} of −0.281. The simulated spectrum thus obtained using the eigenvectors obtained at the B3LYP/6-311++G(3df,3pd) level is shown in Fig. 2(c). The intensity pattern in this spectrum resembles the experimental spectrum quite closely. It is to be mentioned that the intensities of prominent peaks at high-frequency region were reproduced well even though the fit was made using the low-frequency peaks mostly. This means that the harmonic approximation made in the method of Sharp and Rosenstock [33] is adequate in the present case. Intensities of major peaks calculated here are listed in Table 4 and compared with the experimental results.

We carried out Franck–Condon fit using eigenvectors obtained at the HF, MP2, DFT/B3LYP and DFT/BP86 levels with various basis sets. The same value for the C_{22} was used in all the calculations. Good fit was achieved regardless of the eigenvectors used. More importantly, the cation geometries thus determined were very similar regardless of the eigenvectors

Table 5
The equilibrium geometries[a] obtained by using quantum chemical calculation and Franck–Condon fit

Level	Basis set	C=C	C–Cl	CCCl	CCH
Quantum chemical calculation[b]					
B3LYP	6-311++G(3df,3pd)	1.396	1.648	124.5	118.8
B3LYP	6-31 + G**	1.403	1.661	124.7	118.8
BP86	6-311++G(3df,3pd)	1.403	1.655	124.3	119.0
HF	6-311++G(2df,2pd)	1.396	1.639	124.5	118.3
MP2	6-311++G	1.400	1.716	124.9	120.1
	Average	1.400	1.664	124.6	119.0
	Standard deviation	±0.004	±0.030	±0.2	±0.7
Franck–Condon fit[c]					
B3LYP	6-311++G(3df,3pd)	1.409	1.647	124.6	117.6
B3LYP	6-31 + G**	1.409	1.647	124.6	117.5
BP86	6-311++G(3df,3pd)	1.408	1.647	124.6	117.6
HF	6-311++G(2df,2pd)	1.407	1.647	124.6	118.1
MP2	6-311++G	1.408	1.647	124.6	117.7
	Average	1.408	1.647	124.6	117.7
	Standard deviation	±0.001	±0.000	±0.0	±0.2

[a] Bond lengths in Å and bond angles in degree.
[b] Equilibrium geometries determined by direct quantum chemical optimization.
[c] Equilibrium geometries determined via Franck–Condon fit to the MATI spectrum using eigenvectors obtained at various quantum chemical levels.

used. Some of the results are listed in Table 5. Also listed in the table are the geometries obtained by direct quantum chemical optimization. The data obtained by the latter method display significant scatter, 1.396–1.403 Å for the C=C bond length, 1.639–1.716 Å for the C–Cl bond length, 124.3–124.9° for the ∠CCCl bond angle 118.3–120.1° for the ∠CCH bond angle. Corresponding scatter is much less in the data obtained by Franck–Condon fit. For example, the C=C bond lengths lie in the range 1.407–1.409 Å while 1.647 Å was obtained for the C–Cl bond length at all the levels. The results clearly show that the lack of knowledge on correct eigenvectors is not one of the major obstacles in the cation structure determination via Franck–Condon fit.

5. Summary and conclusion

It is very challenging to determine the structure of a gas phase polyatomic cation. Previously, we suggested that the geometry of a cation might be determined via Franck–Condon fit of the corresponding MATI spectrum. A requirement for the validity of this method is that the influence of the channel interaction is not important enough to alter the intensities of major peaks, which is sometimes difficult to determine. Careful analysis of the one-photon MATI spectrum of *cis*-$C_2H_2Cl_2$ obtained in this work showed that the frequencies and intensities looked normal at least for major peaks. Namely, there was no evidence for the major spectral alteration caused by mechanisms such as autoionization and channel interaction. This led us to attempt the cation structure determination via Franck–Condon fit. Even though the eigenvectors for the neutral and cation obtained by quantum chemical calculations had to be used, this does not seem to be a major difficulty because the final results were insensitive to the quantum chemical levels used. The structure of *cis*-$C_2H_2Cl_2^+$ determined by Franck–Condon fit in this work may be regarded as useful benchmark data for the development and test of quantum chemical method to determine the cation structures in the future.

Acknowledgments

Y.J. Bae thanks the Ministry of Education for the Brain Korea 21 fellowship.

References

[1] S. Willitsch, F. Merkt, Int. J. Mass. Spectrom. 245 (2005) 14.
[2] M. Sommavilla, F. Merkt, J. Phys. Chem. A 108 (2004) 9970.
[3] M.S. Ford, X. Tong, C.E.H. Dessent, K. Müller-Dethlefs, J. Chem. Phys. 119 (2003) 12914.
[4] M.C.R. Cockett, Chem. Soc. Rev. 34 (2005) 935.
[5] R. Seiler, U. Hollenstein, T.P. Softly, F. Merkt, J. Chem. Phys. 118 (2003) 10024.
[6] U. Hollenstein, R. Seiler, H. Schmutz, M. Andrist, F. Merkt, J. Chem. Phys. 115 (2001) 5461.
[7] M. Hochlaf, T. Baer, X.M. Qian, C.Y. Ng, J. Chem. Phys. 123 (2005) 144302.
[8] M. Lee, M.S. Kim, J. Phys. Chem. A 110 (2006) 9377.
[9] M. Riese, Z. Altug, J. Grotemeyer, Phys. Chem. Chem. Phys. 8 (2006) 4441.
[10] M. Lee, H. Kim, Y.S. Lee, M.S. Kim, J. Chem. Phys. 123 (2005) 024310.
[11] E.W. Schlag, ZEKE Spectroscopy, Cambridge University Press, Cambridge, U.K., 1998.
[12] C.Y. Ng, Annu. Rev. Phys. Chem. 53 (2002) 101.
[13] S.T. Park, H.L. Kim, M.S. Kim, Bull. Korean Chem. Soc. 23 (2002) 1247.
[14] L. Zhu, P. Johnson, J. Chem. Phys. 94 (1991) 5769.
[15] S.T. Park, S.K. Kim, M.S. Kim, Nature 415 (2002) 306.
[16] S.T. Park, M.S. Kim, J. Am. Chem. Soc. 124 (2002) 7614.
[17] T. Imajo, K. Tokieda, Y. Nakashoma, K. Tanaka, T. Tanaka, J. Mol. Spectrosc. 204 (2000) 21.
[18] F.J. Grieman, B.H. Mahan, A. O' Keefe, J. Chem. Phys. 72 (1980) 4246.
[19] R.C. Woods, T.A. Dixon, R.J. Saykally, P.G. Szanto, Phys. Rev. Lett. 35 (1975) 1269.
[20] M. Ford, R. Lindner, K. Müller-Dethlefs, Mol. Phys. 101 (2003) 705.
[21] R.G. Neuhauser, K. Siglow, H.J. Neusser, J. Chem. Phys. 106 (1997) 896.
[22] Y.J. Bae, M. Lee, M.S. Kim, J. Phys. Chem. A 110 (2006) 8535.
[23] M. Lee, H. Kim, Y.S. Lee, M.S. Kim, J. Chem. Phys. 122 (2005) 244319.
[24] C. Wu, Y. He, W. Kong, Chem. Phys. Lett. 398 (2004) 351.
[25] Y. Xie, H. Su, W.B. Tzeng, Chem. Phys. Lett. 374 (2004) 182.
[26] C.H. Kwon, M.S. Kim, J. Chem. Phys. 121 (2004) 2622.
[27] M. Lee, M.S. Kim, J. Phys. Chem. A 107 (2003) 11401.
[28] S.T. Park, S.K. Kim, M.S. Kim, J. Chem. Phys. 114 (2001) 5568.
[29] C.H. Kwon, H.L. Kim, M.S. Kim, J. Chem. Phys. 118 (2003) 6327.
[30] C.H. Kwon, H.L. Kim, M.S. Kim, J. Chem. Phys. 119 (2003) 215.
[31] J.A.R. Samson, Techniques of Vacuum Ultraviolet Spectroscopy, Wiley, New York, 1967.
[32] M.J. Frisch, G.W. Trucks, H.B. Schlegel, G.E. Scuseria, M.A. Robb, J.R. Cheeseman, V.F. Zakrzewski, J.A. Montgometry, R.E. Stratmann, J.C. Burant, S. Dapprich, J.M. Millam, A.D. Daniels, K.N. Kudin, M.C. Strain, O. Farkas, J. Tomasi, V. Barone, M. Cossi, R. Cammi, B. Mennucci, C. Pomelli, C. Adamo, S. Clifford, J. Ochterski, G.A. Petersson, P.Y. Ayala, Q. Cui, K. Morokuma, D.K. Malick, A.D. Rabuck, K. Raghavachari, J.B. Foresman, J. Cioslowski, J.V. Ortiz, B.B. Stefanov, G. Liu, A. Liashenko, P. Piskorz, I. Komaromi, R. Gomperts, R.L. Martin, D.J. Fox, T. Keith, M.A. Al-Laham, C.Y. Peng, A. Nanayakkara, C. Gonzalez, M. Challacombe, P.M.W. Gill, B.G. Johnson, W. Chen, M.W. Wong, J.L. Andres, M. Head-Gordon, E.S. Replogle, J.A. Pople, Gaussian 98, revision A.6, Gaussian Inc., Pittsburgh, PA, 1998.
[33] T.E. Sharp, H.M. Rosenstock, J. Chem. Phys. 41 (1964) 3453.

[34] K. Kimura, S. Katsumata, Y. Achiba, T. Yamazaki, S. Iwata, Handbook of HeI Photoelectron Spectra of Fundamental Organic Molecules, Japan Scientific Societies Press, Tokyo, 1980, p. 100.
[35] L. Schäfer, J.D. Ewbank, K. Siam, D.W. Paul, D.L. Monts, J. Mol. Struct. 145 (1988) 135.
[36] T. Shimanouchi, Tables of Molecular Vibrational Frequencies Consolidated, vol.1, National Bureau of Standards, 1972, p. 80.
[37] K.C. Lau, H.K. Woo, P. Wang, X. Xing, C.Y. Ng, J. Chem. Phys. 124 (2006) 224311.
[38] W.A. Chupka, E.R. Grant, J. Phys. Chem. A 103 (1999) 6127.
[39] C. Yeretzian, R.H. Hermann, H. Ungar, H.L. Selzle, E.W. Schlag, S.H. Lin, Chem. Phys. Lett. 239 (1995) 61.